Nanoscale

PAPER

View Article Online
View Journal | View Issue

Cite this: *Nanoscale*, 2021, **13**, 10478

The formation mechanism and chirality evolution of chiral carbon dots prepared *via* radical assisted synthesis at room temperature†

Lorenzo Branzi,[a] Giacomo Lucchini,[b] Elti Cattaruzza,[a] Nicola Pinna,[c] Alvise Benedetti *[a] and Adolfo Speghini *[b]

Received 26th March 2021,
Accepted 12th May 2021

DOI: 10.1039/d1nr01927a

rsc.li/nanoscale

We report on a Cu(II) catalyzed process for the production of cysteine based chiral carbon dots; the process does not require any thermal treatment and the carbon dot formation is driven by the production of reactive radical species that are generated in the reaction media by the catalytic role played by the multivalent transition metal. The nanomaterial presents a well-defined chirality and the enantioselectivity of the synthesis is proved by the isolation of both the carbon dot enantiomers. We focused our attention on the processes that take place during the carbon dot formation and the relationship with the structure of the organic starting material. Thanks to the comparison of reactions conducted with different organic substrates whose thiyl radical chemistry is known, we recognized a non-trivial role of the radical hydrogen abstraction reactions in the carbon dot formation process. The reported process allows access to a large variety of analyses to monitor the reaction mixtures during the reaction course. Finally, we report a detailed analysis on the evolution of optical chirality during the synthesis and related this feature with the formation mechanism of the nanomaterial revealing significant evidence on the chirality origin and structure of chiral carbon dots.

Introduction

Carbon quantum dots, also named carbon dots (CDs), are defined as carbon nanoparticles composed of a graphitic or amorphous carbon core and a surface rich in oxygen containing functional groups.[1] Due to their outstanding properties such as simple and low cost production, high photoluminescence, no/low toxicity, and optical and electrooptical properties,[2] CDs are valid candidates for several technological applications such as imaging, sensing and catalysis.[2–9] Further doping with heteroatoms (*e.g.* nitrogen and sulfur) has been shown to affect their surface functionalities and enhance their optical and electrochemical properties.[10]

Recently, the production of CDs with a precise chirality has attracted great interest. Chiral nanomaterials are a promising technological frontier with potential applications in enantioselective catalysis, separation and others.[11] After the first reports about the introduction of chirality in graphene quantum dots through a top-down multi-step process by Suzuki *et al.* and Vázquez-Nakagawa *et al.* in 2016,[12,13] based on the covalent interaction of chiral molecules on the surface of achiral nanoparticles, several authors have investigated alternative pathways *via* single step processes. In the single step process, chiral CDs are directly isolated by the controlled decomposition of an appropriate optically pure organic substrate *via* a bottom-up approach. Amino acids are the most investigated class of chiral starting materials, such as cysteine,[14–20] tryptophan[21] and arginine.[22]

In particular, the controlled decomposition of optically pure cysteine produces CDs with a well-defined chirality and, at the same time, guarantees an adequate heteroatom doping (S,N-doped CDs). The synthesis based on hydrothermal or electrochemical approaches has stimulated several investigations. After the first evidence on the enantioselective recognition of L- and D-tartrate reported by Kang's group,[14,15] by electrochemical impedance spectroscopy and linear sweep voltammetry, the applications of chiral CDs obtained from cysteine have been extensively investigated in biochemistry. Li *et al.*[18] reported the effect of chiral CDs on the cellular energy metabolism of human bladder cancer T24 cells, Zhang *et al.*[17]

[a]*Department of Molecular Sciences and Nanosystems, Ca' Foscari University of Venice, Via Torino 155, Venezia Mestre, Italy. E-mail: benedett@unive.it*
[b]*Nanomaterials Research Group, Department of Biotechnology and INSTM, RU of Verona, University of Verona, Strada le Grazie 15, Verona, Italy. E-mail: adolfo.speghini@univr.it*
[c]*Institut für Chemie and IRIS Adlershof, Humboldt-Universität zu Berlin, Brook-Taylor-Str. 2, 12489 Berlin, Germany*

†Electronic supplementary information (ESI) available. See DOI: 10.1039/d1nr01927a

monitored their reaction on mung plant growth, Hu *et al.*[16] analysed their effect on the activity of laccase enzyme and Li *et al.*[19] investigated the CD capability to mimic the role of topoisomerase I enzyme in the rearrangement of supercoiled DNA into the nicked open circular DNA. Finally, Victoria *et al.*[20] focused on their microbial activity against various strains of Gram-positive and Gram-negative bacteria.

In the last years, many efforts have been made to investigate CD formation *via* the bottom-up approach and a review on this topic was recently published.[23] The study on the formation mechanism of CDs, based on citric acid and a mixture with amine (such as ethanolamine[24,25] and ethylenediamine[26]), clarified some critical aspects on carbon dot formation. It is generally accepted that organic substrates are transformed into polymer amorphous dots that further evolve into graphitic CDs in a longer reaction time or at a higher reaction temperature. The study of CD photoluminescence (PL), and the comparison with molecular fluorophores, have suggested a core–shell model, in which a graphitic PL-silent core is surrounded by an amorphous shell that contains luminophores.[23] Although it is only supported by few investigations, this model has also been proposed for chiral CDs made up of a graphitic core surrounded by an amorphous chiral shell. The evidence reported by Đorđević and co-workers,[22] on the microwave decomposition of an optically pure arginine and 1,2-cyclohexanediamine mixture, shows that L-arginine completely decomposes, losing its chirality and contributing to the formation of an achiral CD core. Chiral CDs can be produced if the decomposition is performed in the presence of optically pure 1,2-cyclohexanediamine, which can retain their chirality even at high temperature. Wei *et al.*[21] established that, in tryptophan based CDs, the chirality arises on partially undecomposed tryptophan structures present on the particle surface. Some evidence on the chirality origin in cysteine based CDs has been reported by Hu *et al.*, and Victoria *et al.*[16–20] observed a considerable reduction of the chiroptical signal when the time or temperature in the synthesis is increased.

Even though some phenomenological evidence has been published, experimental observations on the formation mechanism of amino acid-based CDs as well as the chirality evolution are still missing. Probably, this is partially related to the synthetic strategy generally used. As a matter of fact, cysteine-based CDs are usually prepared by thermal decomposition of optically pure cysteine under hydrothermal conditions. The reaction in autoclaves or microwave reactors imposes serious issues on the *in situ* investigations on the formation process.

Motivated by great interest on cysteine-based CDs, we developed a novel room temperature synthesis based on copper catalysis. The process leads to the decomposition of cysteine within a few hours and without any thermal treatment. This is particularly suitable for "*in situ*" measurements during cysteine decomposition. It is well known that cysteine is involved in several radical processes that have significant roles in biochemistry, especially in protein oxidative damage.[27,28] The formation of the cysteine oxidized dimer (cystine) can be efficiently catalysed by multivalent transition metals such as iron and copper.[29] The catalytic process can form several radical species, and, among them, reactive oxygen species (ROS) and reactive sulfur species (RSS), such as thiyl radicals, under specific conditions can take part in the CD formation process.

We herein present a bottom-up approach for the synthesis of cysteine-based chiral CDs at room temperature. The reported process is based on the reactions between copper(II) salts and cysteine in alkaline solution (pH = 10.5). The catalytic reaction produces radical species that take part in the CD formation process without any thermal treatment. The isolation of both the CD enantiomers, by changing the starting material isomer, proves the enantioselectivity of the synthesis. The morphology and optical properties of the chiral CDs obtained by this method were extensively analysed. Finally, we investigated the reaction mechanism through different spectroscopic techniques and we observed some structure–reactivity relationships that could be useful for further application of radical assisted methods in CD synthesis.

Results and discussion

Cysteine based chiral CDs have been prepared by copper catalysed radical assisted decomposition. As shown in Fig. 1, at pH 10.5, the addition of 4%$_{mol}$ of Cu(II) acetate in an optically pure cysteine solution forms L or D CDs after 2 h. Due to its simplicity, the process is suitable for scaling up to a larger extent. Salts and other by-products can be eliminated during the purification step and carbon dots on a gram scale can be isolated. The characterization studies are focused on **L-CDs** prepared by the decomposition of L-cysteine. **D-CDs** are also isolated to confirm the enantioselectivity of the synthesis.

The TEM micrographs of the **L-CDs** shown in Fig. 2 and Fig. S1† display nanoparticles with an average size of 6 ± 2 nm. The phase contrast images (Fig. 2c and d) show the diffraction fringes of the graphitic core. From the analysis of the fringes, the *d* spacing of 0.19, 0.22 and 0.31 nm is measured and can be related to the 101, 100 and 002 facets of the graphitic CD core. Further details on the diffraction pattern can be seen from the Fourier filtered image in Fig. 2e, which shows the expected hexagonal pattern. The selected area electron diffraction (SAED) analysis of an assembly of CDs reveals the Debye–Scherrer rings, typical of a polycrystalline sample (Fig. 2f). The powder X-ray diffraction (PXRD) pattern shown in Fig. S2† shows a very broad signal ascribed to a structure rich in struc-

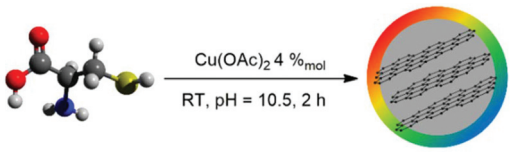

Fig. 1 Scheme of the synthesis conditions for the preparation of L-CDs from L-cysteine.

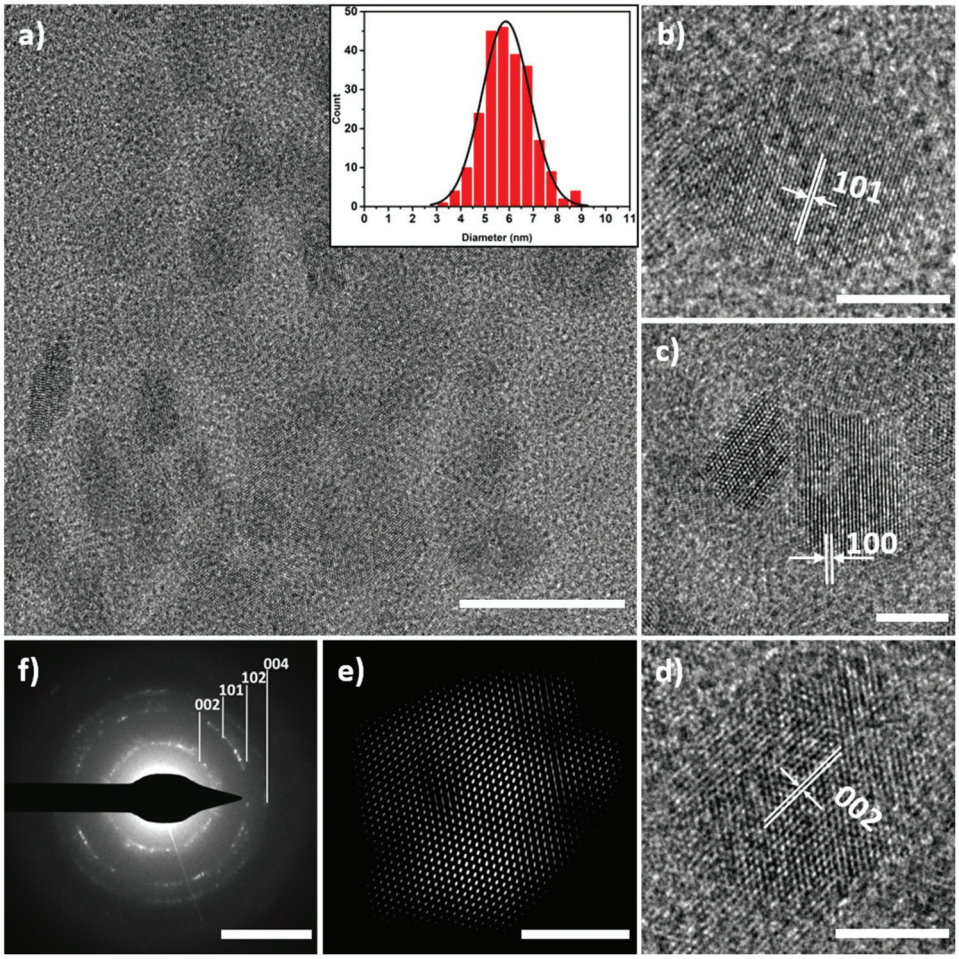

Fig. 2 TEM analysis of **L-CDs**: (a) a low magnification image, particle size distribution 6 ± 1 nm, scale bar: 10 nm. (b–d) Phase contrast images, scale bar: 5 nm. (e) Image d after the application of a Fourier filter, scale bar: 5 nm. (f) SAED analysis, scale bar: 5 nm^{-1}.

tural defects. A signal centred around 28°, corresponding to 0.32 nm, is ascribed to the *d*-spacing of the (002) plane of the graphite lattice, a feature commonly observed in CD samples.[16]

The surface functional groups of **L-CDs** are investigated by Fourier transform infrared spectroscopy (FTIR), in comparison with zwitterionic L-cysteine (Fig. 3a and b). The identification of the absorption bands of zwitterionic L-cysteine is based on the detailed experimental and computational analyses reported by Pawlukojć and co-workers[30] about the structure, and Raman and IR active modes of L-cysteine. The absorption of **L-CDs** shows many common features with those of L-cysteine, even if all the bands are broader and some signals are significantly modified: the wide region related to the absorption of the amine groups is blue shifted to the 3800–3300 cm^{-1} range, a feature associated with the formation of amidic bonds. This attribution is further supported by the observation of ν_{CO}^{amide} at 1700 cm^{-1} (amide I band) and the strong absorption related to the amide II band at 1590 cm^{-1}, as well as the absence of absorption bands related to $-NH_3^+$ (although the product is isolated under acidic conditions, see the Experimental section). In the product, a band at 1465 cm^{-1} appears and it is associated with C=C stretching in the aromatic structures produced during the decomposition. The bands in the 1400–1370 cm^{-1} range can be related to C–N stretching modes. The band related to the δ_{SH} mode located at 943 cm^{-1} in the L-Cys spectrum disappears in the product, suggesting the inclusion of sulfur as C–S–C or the oxidation to sulfoxide derivatives (such as cysteic acid and taurine), as observed by the presence of the absorption at 1020 cm^{-1} of SO_3^- and further confirmed by the XPS analysis (see below).[31]

The UV/Vis spectrum presented in Fig. 3c shows a wide and diffuse absorption with no well-defined absorption band and the presence of a shoulder at about 280 nm. The absorption below 250 nm can be associated with the $n \rightarrow \pi^*$ transitions in the amidic and carboxylic bonds and with transitions in the graphitic core. However, the shoulder at 280 nm and the absorption at a higher wavelength are ascribed to the $\pi \rightarrow \pi^*$ transitions in the surface aromatic and heteroaromatic groups. The photoluminescence excitation (PLE) analysis reveals that the luminescence is derived mostly by luminophores absorbing in the 300–450 nm range, with a maximum that is strongly

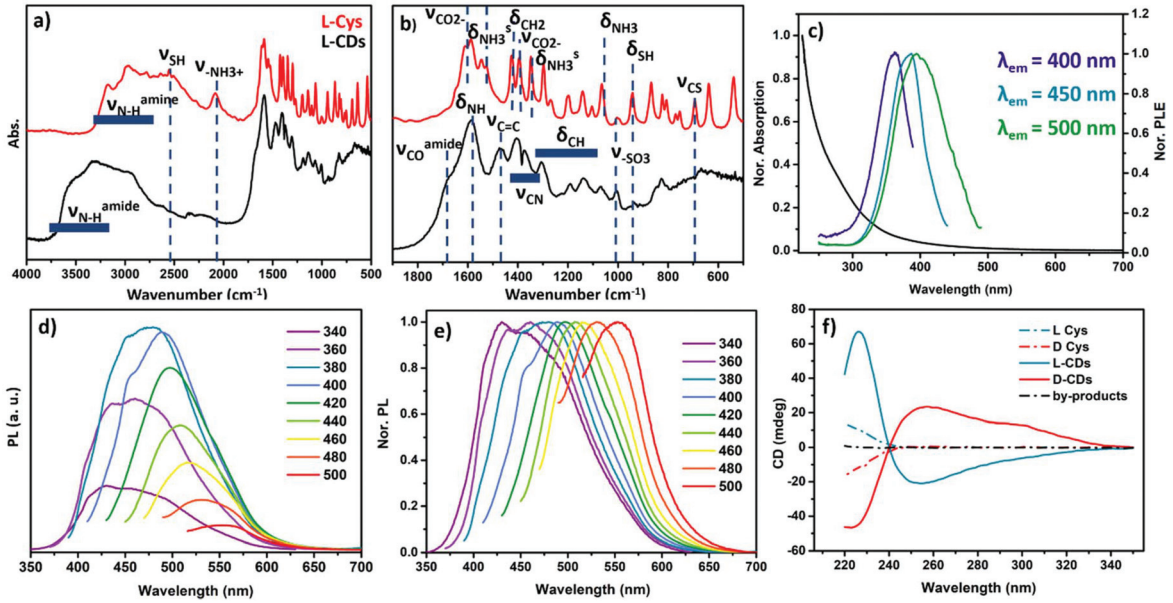

Fig. 3 Characterization of **L-CDs**: (a and b) FTIR analysis and detail of the analysis in the 1900–500 cm^{-1} range. (c) UV/Vis and PLE spectra recorded at 400, 450 and 500 nm emission wavelengths. (d and e) PL and normalized PL spectra recorded at different excitation wavelengths. (f) Electronic circular dichroism of L,D-cysteine, **L,D-CDs** and the by-product.

red shifted as a function of the collected wavelengths in the 400–450 nm range, highlighting the presence of a heterogeneous population of a photoluminescent species. This feature is further confirmed by the strong effect of the exciting radiation energy on the emission properties, as shown in Fig. 3d and highlighted in Fig. 3e by the normalized PL spectra. The **L-CD** emission has a maximum intensity between 400 and 500 nm, which corresponds to the excitation wavelengths in the 360–400 nm range. Three main components of the emission profiles were centred at 415, 455 and 500 nm, respectively, and assigned to the broad families of luminophores with different conjugation extentions[32] or heteroatom doping.[33] We have measured the photoluminescence quantum yield (PLQY) using an exciting radiation at 350 nm, considering quinine sulfate as a reference. The obtained PLQYs for the L-CD samples dispersed in deionized water and 0.1 M H_2SO_4 solution are 0.8% and 1.5%, respectively (see Table S1 in the ESI†). These values are in line with those obtained for similar cysteine based CDs.[34]

The chirality of **L-CDs** is confirmed by electronic circular dichroism (ECD) analysis (Fig. 3f); **L-CDs** show a strong positive ECD signal at 222 nm and a negative signal at 250 nm that can be associated with the n → π* transition in the amidic bonds and the π → π* transition that derives from the aromatic superficial groups, respectively. The formation of the new optically active chromophores during the reaction is evidenced by the absorption in the 240–340 nm range, where no L-cysteine signal can be detected. According to the literature, L-cysteine shows a positive maximum at 206 nm. Under our experimental conditions, as shown in Fig. 3f, only the tail of the signal can be observed.[35] Probably, the surface of the **L-CDs** still contains some cysteine molecules (or cysteine derivatives), grafted through the amidic bond, that preserve the chiral information in C_α and are responsible for the absorption at 222 nm. And, the absorption at 250 nm could be ascribed to aromatic systems that are in local proximity of the stereocenter and, consequently, the electronic transitions of these groups are influenced by the effect of the asymmetric groups. The **D-CD** sample is prepared by radical decomposition of D-cysteine solution. The ECD signal, shown in Fig. 3f, confirms the isolation of the other enantiomers and the enantioselectivity of the synthetic protocol.

The relative elemental analysis of **L-CDs** is performed by XPS starting from the peak area of the single signals (Fig. 4)

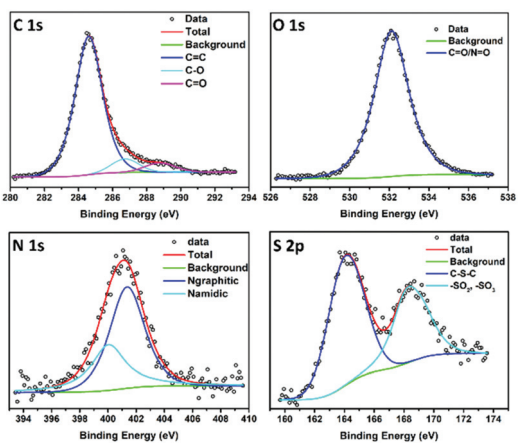

Fig. 4 XPS spectra of: C 1s, O 1s, N 1s and S 2p peaks of **L-CDs**.

corrected by the elemental sensitivity factors. The composition, related to the typical XPS sampling depth of 5–10 nm, is C 68.7%, O 23.5%, N 4.1% and S 3.7%. The deconvolution of the C 1s signal shows three different components: the most intense component is centred at 284.6 eV and can be assigned to the carbon–carbon bonds related to the graphitic core in nanoparticles and possibly in aromatic structures; and the two other low intensity components, centred at 286.6 eV and at 288.5 eV, can be due to the oxidation of carbon, existing in the C–O/C–N and C═O/C═O–N bonds, respectively.[36] The O 1s band can be well fitted by using only one component, centred at 532.1 eV. This BE position can be attributed to the C═O/N═O bonds,[16] and possibly also to the sulfur–oxygen bonds. We cannot exclude the presence of some weak components due to the C–O bonds in the O 1s band. The deconvolution of the N 1s peak shows that the signal is composed of two components centred at 399.8 and 401.3 eV: they can be ascribed to nitrogen involved in the amidic bonds and nitrogen included in the graphitic structures, respectively.[33] The S 2p signal shows the presence of two well-distinct components, centred at 163.8 eV and at 168.1 eV, respectively: the first is related to sulfur atoms in a low oxidation state (as for instance the C–S–C groups) and the second is related to sulfur in high oxidation states such as sulfenic and sulfonic acids and their derivatives, $-SO_2$ and $-SO_3$.[16,37]

During the purification process, it is possible to isolate a carbonaceous by-product (see the Experimental section) that corresponds to around 10% of the product mass, since this fraction is composed of larger carbonaceous materials (up to a few micrometers, Fig. S3†), which does not show any chiroptical activity (Fig. 3f), and the optimization of the reaction conditions does not allow to further reduce its amount; this fraction is removed by all the products during the purification step. Moreover, in order to obtain a complete view of the process that leads to the formation of **L-CDs** by copper catalysed oxidation of cysteine, we also isolated, purified and analysed this fraction (see the ESI, Fig. S3–6†).

Based on the reported characterization studies and the core–shell model of the structure of bottom-up CDs suggested by other works, in Fig. 5, we report a schematic structure of our CDs. The main reaction products are CDs with an achiral graphitic core of 6 nm as shown in Fig. 2 by the TEM analysis.

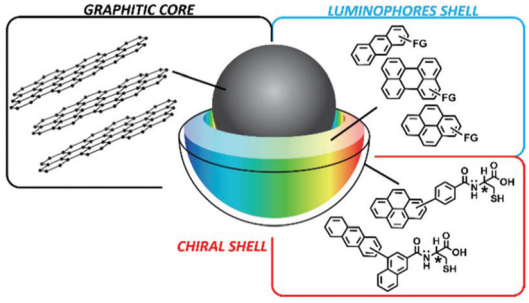

Fig. 5 General scheme of the Cys-based CDs.

The core is surrounded by an amorphous shell that contains the luminophores, probably a heterogeneous family of conjugated structures, rich in heteroatoms confined by the sp^3 regions. The structure of this shell gives rise to broad absorption and emission dependent PL as suggested by Fu *et al.*[32] in their experiment on the origin of excitation-dependent PL of CDs. Finally, the chirality probably originates from undecomposed cysteine or derivatives grafted by the amide bond forming a "chiral shell", as suggested by our experimental evidence (ECD and FTIR analysis, Fig. 3), and by Wei *et al.*[21] on the formation of chiral CDs from tryptophan.

Investigation on the formation mechanism

State of the art

Since the first observation at the beginning of the XXth century,[38] the process of Cu(II) catalysed self-oxidation of cysteine can be considered of remarkable significance in the research on the oxidative decomposition of biologically active thiols, involving many researchers in the investigation of the mechanism and kinetics. The self-oxidation of thiols is mainly described by eqn (1) and (2) in Scheme 1. The formation of disulfide results in the production of water or hydrogen peroxide. The formation of other reactive sulfur species such as sulfenic, sulfinic and sulfonic acids was also considered and the amounts of the different products were mainly related to the pH.[39]

Due to the wide scientific interest in biomolecule decomposition under oxidative stress conditions, copper catalysed self-oxidation of cysteine was extensively investigated by several authors. The investigation at pH = 7.4 by Pecci *et al.*[40] evidenced the active role of a Cu(I) bis–thiol complex in the catalytic cycle, and Rigo *et al.*[41] investigated the formation of Cu(I) complexes by ^{1}H-NMR, following the titration of cysteine solution with Cu(I) and Cu(II) solutions. Several details on the reaction mechanism have been reported by Buzuk *et al.*[42] by monitoring the Cu(II) concentration with a Cu ion selective electrode (ISE) during the oxidation process. The observations of the coordination role of the thiol molecules were reported by Bagiyan and co-workers.[43] They compared the kinetic characteristics of a wide pool of thiol compounds and related their activity to different chelating capabilities. In particular, they divided the investigated pool into three groups: non-chelating, weakly chelating and chelating (cysteine, glutathione and cysteamine are some examples of this third class). The analysis of the oxygen and hydroxyl radical concentrations in solution during the oxidation process, reported by Kachur *et al.*,[29]

1) $2\,RSH + O_2 \rightleftharpoons RSSR + H_2O_2$
2) $4\,RSH + O_2 \rightleftharpoons 2\,RSSR + 2\,H_2O$

Scheme 1 Overall reactions of the thiol RSH self-oxidation into its disufide dimer RSSR.

revealed the presence of two distinct phases active separately in the self-oxidation process: phase (i) – free cysteine is still present in solution and it can take part in the metal binding; in this phase, the oxygen consumption can be related to the oxidation of cysteine into cystine and the concentration of hydroxyl radicals is still low; and phase (ii) – when there is no longer free cysteine in solution; in this second phase, the oxygen consumption increases due to the activity of reactions that convert cysteine into sulfinic and sulfonic acids with an increase of the hydroxyl radical concentration. Moreover, they recognized the different behaviours between cysteine and cysteine derivatives (*N*-acetylcysteine, cysteamine and cysteine ethyl ester) and correlated the different capabilities of the thiol compounds to bind to the metal centre in relation to the thiol/Cu ratio observed at the beginning of the second phase.

Cavallini *et al.* investigated the catalytic cycle at alkaline pH. They observed the catalytic oxidation and recognized a fundamental intermediate that takes part in the catalytic self-oxidation cycle.[44] This species is characterized by an intense absorption band at 330 nm and a shoulder at 390 nm, and for this feature, it was named the "330 compound". The compound is stable in the presence of oxygen and its concentration in solution remains constant until all the free cysteine is consumed. The EPR analysis of frozen solutions evidenced the paramagnetic nature of the "330 compound". By spectrophotometric titration, a 1 : 2 ratio of Cu(II) : thiol was evaluated, and a Cu(II) coordination complex with two molecules of cysteine has been proposed. The author suggested that the transfer of one electron from the thiol to the molecular oxygen could occur in two distinct steps: the first from cysteine to Cu(II) giving the formation of thiyl radicals and the metal in the reduced form and the second from Cu(I) to oxygen with the formation of a superoxide radical ion and the oxidation of the metal centre. Since in alkaline solutions, the second step is faster compared to the first one, the copper is mainly observed in the oxidized Cu(II) state. Since the investigation on the details of the mechanism of the copper catalysed self-oxidation of cysteine is outside the scope of this work, we present in Scheme 2 a simplified picture of the role of the metal centre in the process.

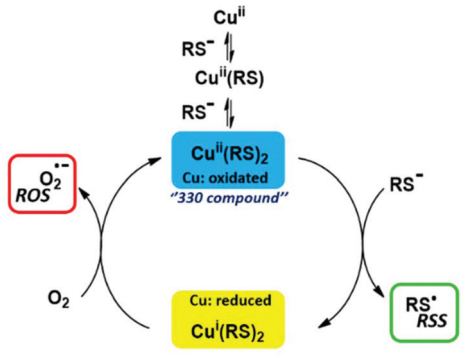

Scheme 2 Representation of the copper role during the catalytic self-oxidation cycle of thiols.

Experimental observations

In order to investigate the processes that take place during the CD formation, several experiments changing the pH or the organic substrate were performed, as reported in Table S2.† The processes that occurred in the reaction mixtures were investigated by ^{1}H-NMR and UV/Vis spectroscopy.

The ^{1}H-NMR analysis of the reaction at pH = 7.0 (Fig. 6a) shows a complex signal between 4.00 and 3.97 ppm ascribed to the H_α proton and the signal between 3.15 and 2.99 ppm ascribed to the methylene protons in the lateral chain (H_β). Both the signals are produced from cysteine. The signals from cystine, indicated in the figure with an asterisk, can be observed also before the copper addition (Fig. S7†) due to the cystine impurity present in commercial cysteine.[41] After the addition of Cu(II), the analysis shows an increase of these signals that can be related to the catalytic role of the metal ion in the aerobic "self-oxidation" of cysteine. The activities of the metal centre are mainly ascribed to its roles as a mediator in the electron transfer between thiol and oxygen and in the dismutation of hydrogen peroxide in Fenton-like reactions.[29] Recently, kinetics analyses conducted by Bagiyan *et al.*[39] evidenced that Cu(II) is more active than other variable-valence metals such as Mn, Fe, Ni and Co in the catalytic oxidation of thiols.

At pH 10.5, in contrast to the observation at pH = 7.0, the formation of cystine is not observed (Fig. 6b). The cysteine signals become broad, and after 60–90 min, all the signals from the organic substrate disappear. This behaviour is not in agreement with the observations reported by Cavallini *et al.* about the interaction between Cu(II) and cysteine at alkaline pH.[44] However, the formation of the "330 compound" in our reaction system can be evidenced by UV/Vis spectroscopy (Fig. 6c). After the addition of Cu(II) acetate, the solution turns yellow and strong absorptions at 330 and 390 nm can be observed. In agreement with Cavallini and co-workers, the absorption of these bands remains constant until all the free cysteine is consumed (around 30 min). Then, in agreement with the second phase, the Cu(II) mono-cysteine complex is reduced intramolecularly to Cu(I) and cysteine thiyl radical.[29] At longer reaction times, the absorption at 280 nm related to the $\pi \rightarrow \pi^*$ transition, as well as to the broad absorption in the visible region, evidencing that this is related to the formation of CDs.

The observation of the "330 compound" confirms the presence of the active species that are involved in the Cu(II) cysteine self-oxidation cycle, and it suggests the formation of several radical reactive species such as RSS (thiyl radicals and disulfide radical anions) and ROS ($O_2^{\bullet-}$, $HO^\bullet$, $HOO^\bullet$ and H_2O_2). However, other processes, different from the cystine formation, can lead to the decomposition of organic substrates, probably due to the specific reaction conditions (pH and concentrations). By FTIR, TEM and XPS analyses of the products reported above, we observed the formation of sulfoxides and

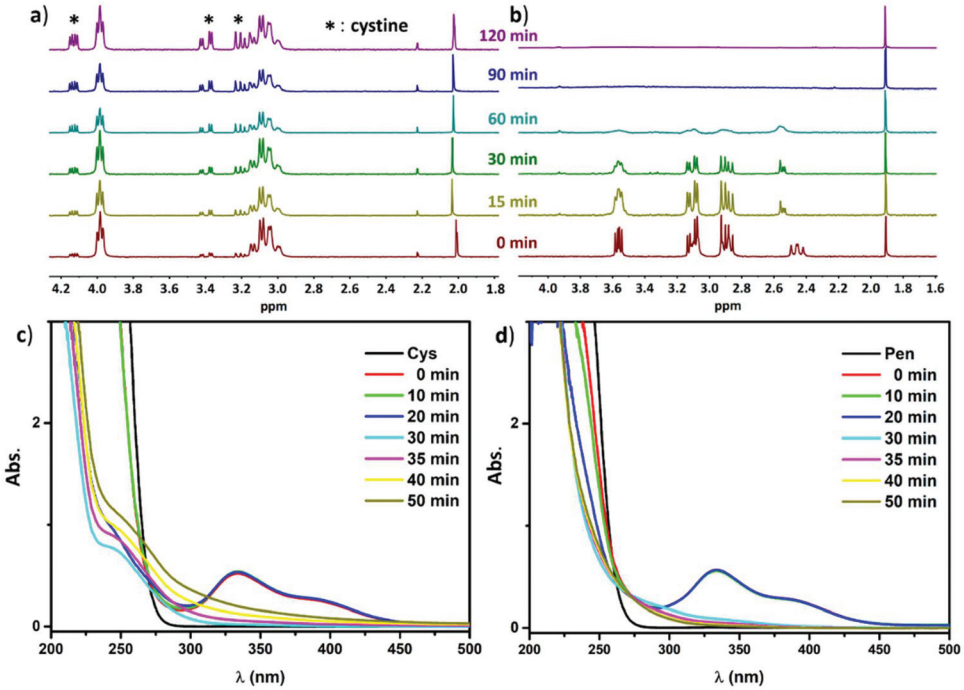

Fig. 6 ^{1}H-NMR analysis of the reaction with L-cysteine at pH 7.0 (a) and 10.5 (b). UV/Vis absorption analysis of the decomposition process of L-cysteine at pH = 10.5 (c) and L-penicillamine at pH = 10.5 (d).

conjugated structures that can be related to the action of several radical species that are generally produced during the catalytic cycle, such as ROS and RSS, which can take part in the formation process of CDs.

In agreement with other studies on the chemistry of thiyl radicals, the sulfur radical is in equilibrium with carbon-centred radicals through 1,2 and 1,3 radical hydrogen transfer reactions (Scheme 3). Zhao *et al.*[45] measured the kinetics of radical proton transfer in several substrates such as cysteine, glutathione and homocysteine by pulse radiolysis. They suggested an intramolecular mechanism that passes through a cyclic transition state. These findings have been confirmed by further studies at acidic pH by Nauser *et al.*[37] on cysteine, cysteamine and penicillamine with the determination of equilibrium and kinetic constants.

The hypothesis that the equilibrium between thiyl and carbon-centred radicals could play a fundamental role in CD formation is supported by the pH dependence: at pH = 10.5, the amine group is mainly present in its neutral form and the electron density of the lone pair in the nitrogen atom could increase the stability of the vicinal C_α captodative radical. The formation of the C_α radical is thermodynamically favourable under these conditions; meanwhile, this process is suppressed at a lower pH.[37] In an oxidized solution, carbon centred radicals are readily converted into peroxyl radicals that lead to the formation to α-imino acids and superoxide radicals in accordance with the investigation reported by Abramovitch and Rabani.[46]

To further validate this hypothesis, we have investigated the behaviour of different substrates with similar proton dissociation constants and structural elements (functional groups and protons involved in the radical hydrogen transfer reactions, H_α and H_β). Cysteine, penicillamine, cysteamine, methionine, thioglycolic acid and glycine (Fig. 7) have been investigated under the same reaction conditions (Table S2†). Based on our observations, the organic substrates can be divided into three categories.

Class I: glycine, thioglycolic acid and methionine. This class of organic substrates cannot stabilize Cu(II) and the formation

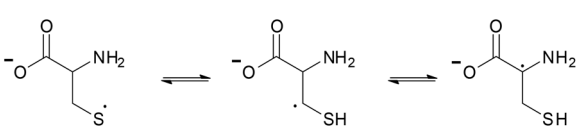

Scheme 3 Equilibrium of thiyl radicals with carbon centre radicals on C_α and C_β in the anionic form of cysteine.

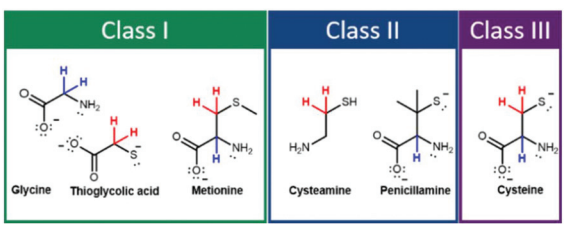

Fig. 7 Structure of the different organic substrates considered in this investigation, H_α and H_β are represented in blue and red, respectively.

of the "330 compound" is not observed. The reaction with a mixture of glycine and TGA 1 : 1 contains both the protons in the glycine C_α position (H_α) and the protons in the thiol vicinal position C_β (H_β) (entries 1–3); the process follows a completely different pathway and the formation of the "330 compound" is not observed after the addition of Cu(II) acetate (Fig. S8†). The same behaviour is observed by the reaction with methionine (entry 4), whose thioether group precludes the interaction with the metal centre as the anionic binding site. We think that the multidentate (κ-S, κ-N) binding mode and the dianionic electronic state of cysteine are necessary for the stabilization of the metal oxidized state.

Thus, the scission of thiol and amine functions or the protection of the thiol group in methionine affect significantly the capability of the organic species that are present in solution to stabilize the Cu(II) oxidation state. Probably, in entries 2 and 3, the metal is rapidly reduced to Cu(I) by thioglycolic acid. This hypothesis is supported by the formation of a transient violet color during the copper addition, a feature that was ascribed to the formation of mixed valence compounds. EPR and stopped-flow UV/Vis investigation on this process were reported by Hanaki Akira.[47]

Class II: penicillamine and cysteamine. These molecules show the formation of the "330 compound" after the Cu(II) addition. However, the CD formation is heavily influenced by the presence of only one group of acidic protons on the organic substrate: H_α penicillamine and H_β cysteamine. As expected, penicillamine (entry 5) is able to bind to the metal centre and stabilize the copper oxidation state. The formation of the "330 compound" can be recognized by the peculiar absorption bands at 330 and 390 nm in Fig. 6d. As observed for the reaction with cysteine, after 20–30 min, almost all the free penicillamine is consumed and the bands at 330 and 390 nm disappear. However, in contrast to the reaction with cysteine, the increase in the absorption at 280 nm related to the $\pi \rightarrow \pi^*$ transitions, the absorption in the visible range, due to the formation of aromatic and heteroaromatic superficial groups, and any luminescence properties are not observed. The ^{1}H-NMR analysis (Fig. S9†) shows that, even if chromophore groups are not produced during the reaction, the organic substrate is completely decomposed by the process. As observed for cysteine, the signals of the organic substrate became broad and lost intensity. Based on the UV/Vis spectroscopy analysis (Fig. 6d), we suggest that the reaction forms a heterogeneous intermediate with a non-regular polymeric structure rather than CDs. Moreover, the ^{1}H-NMR analysis shows that the amount of the oxidized disulfide dimer increases in the first 60 min of reaction. Probably, this effect is due to the higher chemical stability of penicillamine disulfide than cystine. Cavallini *et al.*[44] investigated the reaction between Cu(II) and cysteamine in alkaline solutions and they observed the formation of the "330 compound" characterized by a faster decomposition than for cysteine. This behaviour is also confirmed by our results (entry 6). Fig. S10† shows a small signal that can be related to the formation of the "330 compound" with cysteamine, but the intensity is not comparable with cysteine or penicillamine findings. The signals remain constant for around 10 min after the decomposition of the "330 compound", and then the absorbance, at a longer wavelength, starts to increase in contrast to the other substrates, suggesting the formation of chromophores. The ^{1}H-NMR analysis of the reaction with cysteamine (Fig. S11†) shows that the process proceeds slower than the reactions with cysteine and penicillamine. The signals observed at 2.92 ppm and 2.80 ppm, at the moment of copper addition, are ascribed to the methylene protons attached to nitrogen and sulfur, respectively. After 30 min, the signals from both the methylene protons lose their hyperfine structure, and the signal at 2.92 ppm becomes broad and it is upshifted to 3.0 ppm after 90 min. Both signals completely disappear after 24 h, and only broad signals, ascribed to the Cu complex with the remaining cysteamine or cysteamine derivatives or heterogeneous species, can be observed.

Since cysteine and penicillamine present similar structures and proton dissociation equilibria, we have considered that the processes involving the carboxyl and the amine functional group, as well as the formation of captodative radicals on the C_α, are comparable for both the substrates. Therefore, the different behaviours of penicillamine could be ascribed to the presence of the two methyl groups in the C_β position. The substitution of these hydrogens has the consequence of preventing the 1,2 radical hydrogen transfer reaction, as observed in precedent studies.[37] The evidence on the formation of chromophores when the reaction involves cysteamine further validates this hypothesis. However, the decomposition of cysteamine solution is slower than those of cysteine and penicillamine and only a pale luminescence can be observed when the solution is irradiated with a 365 nm lamp, suggesting the low efficiency of the processes involved in the CD formation. This feature can be related to the different stabilization capabilities of the oxidized metal form. Kachur *et al.*[29] observed that the second phase of the self-oxidation cycle of cysteine derivatives started earlier than what was observed with cysteine, they related this behaviour to the different binding modes.

Class III: cysteine. As already discussed, cysteine (entries 7–9) forms the "330 compound" after the addition of copper (Fig. 6c), and the organic substrate is readily converted into CDs after a few hours (Fig. 6b). Therefore, we can conclude that several structural features, characteristic of the cysteine molecule, are in some way fundamental for the participation of the organic substrate in the radical assisted formation process. In particular, we recognized the synergistic roles played by: (1) the free thiol group that can interact with the metal centre and take part in the redox reactions with the formation of radical species. (2) Aminic and carboxylic functional groups that complete the binding mode with the metal and control the electron density on the metal centre as well as the stability of the oxidized state. (3) Hydrogen atoms that can take part in the radical hydrogen transfer reactions (H_α and H_β) and give the formation of carbon centred radicals. In particular, the observations with penicillamine highlight the dramatic role of H_β in the formation of luminophores.

Chirality evolution during the CD formation

The evolution of the chiroptical signal during the cysteine decomposition is investigated by collecting the ECD spectra of 1 ml of the reaction mixture at different reaction times. The reaction is quenched before the analysis with the addition of 20 μL of 2 M HCl solution and the by-product is removed by centrifugation (5000 rpm for 5 min). The ECD analysis in Fig. 8a and b shows a rapid increase of the CD signal characterized by a maximum at 219 nm and a minimum at 250 nm, with a maximum intensity around 1.5 h remaining almost constant until 2 h. For a longer reaction time, see Fig. 8b, the intensity of the ECD signal decreases progressively. In order to correlate these observations with the evolution of the nanoparticle structure, the absorption in the UV/Vis region and the photoluminescence properties of the samples are analysed. The UV/Vis spectroscopy analysis presented in Fig. 9 shows the progressive evolution of the chromophores on the CD surface. Furthermore, the samples collected within 2 h of the reaction show considerable absorption at 250 nm. The intensity of this band increases until 1.5 h and becomes almost constant at 2 h. Based on the time dependence and position of this absorption band, we considered that it can be ascribed to the chiroptical active chromophores present in the CDs. At longer reaction times, the formation of other achiral chromophores are favoured: strong absorptions at 270, 325 and 390 nm appear after 8 h and their intensities increase with the reaction time. The PL investigation (Fig. S12–14†) covers both different pH values and excitation wavelengths for the complete optical characterization of the CD formation process. We did not observe any significant luminescence for the samples collected at reaction times shorter than 0.5 h; in this phase, the cysteine decomposition is not completed and the formation of luminophores is not active yet. Instead, a constant increase in the PL intensity is observed for the sample collected at a longer reaction time. Since the samples collected after 2 h and 84 h show similar values of the PLQY (around 1.5%, see Table S1†), we relate the variation of the PL intensity to the increase of the concentration of luminophores on the nanoparticle surface.

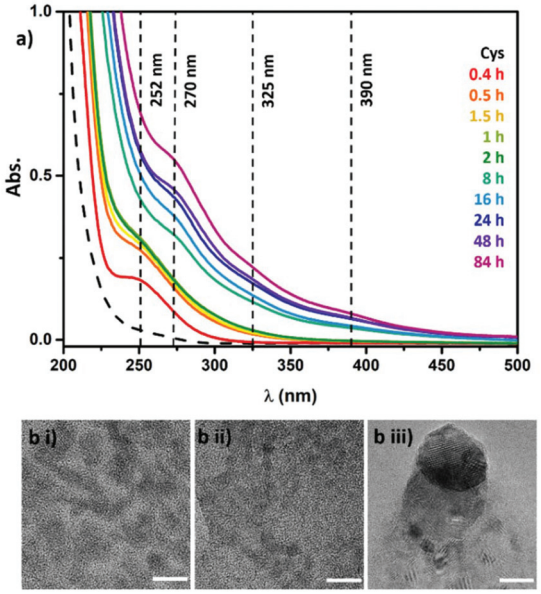

Fig. 9 (a) UV/Vis spectra of the fractions collected at different reaction times. (b) TEM micrographs of the **L-CDs** after purification isolated at (i) 2 h (ii) 48 h and (iii) 84 h; the scale bars i–iii correspond to 10 nm.

For the sample collected in the 0.5–2 h range, a strong pH dependence is observed. In particular, samples collected after 0.5 and 1 h show more intense emission related to luminophores excited at 350 nm at pH 2 and pH 7; meanwhile, at alkaline pH, the components that absorb at 375 nm are more active. This behaviour is gradually lost at a longer reaction time and it is ascribed to the evolution of luminophore species that show a lower pH dependence, probably due to the consumption of vicinal functional groups that are affected by protonation equilibria and can act as quenchers for the luminophores. Intermediate molecular-like luminophores can be observed in the sample collected in the 0.5–1.5 h range, indicated by the high symmetrical and excitation independent

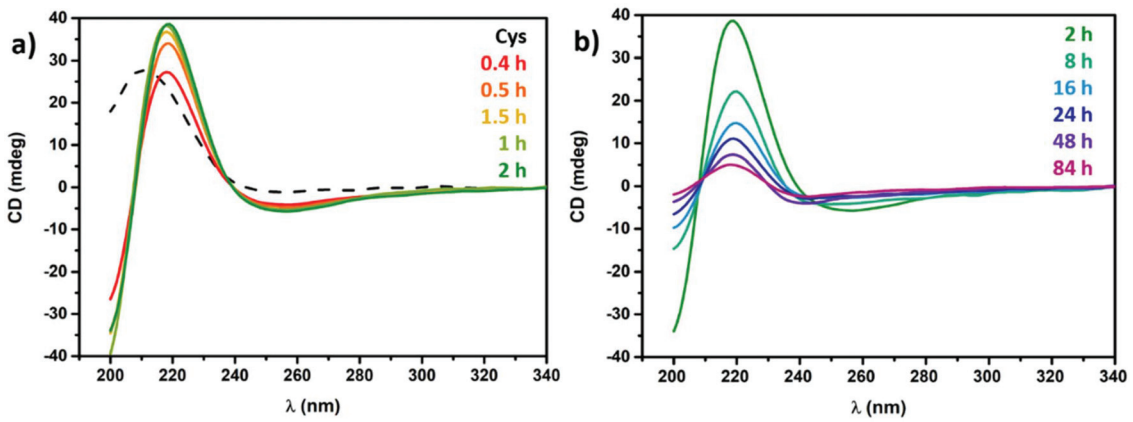

Fig. 8 Evolution of the chiroptical signal during the reaction period: (a) 0–2 h and (b) 2–84 h.

emission at 550 nm at pH 2 and at pH 7 when excited at around 500 nm. This species is further consumed for a longer reaction time.

The morphologies of the samples collected at 2 h, 48 h and 84 h are characterized by TEM analysis (Fig. 9b and Fig. S15–17†). The samples collected at 2 h and 48 h show the presence of well-separated nanoparticles, with an average diameter of around 6 nm for 2 h and slightly smaller, around 5 nm, for 48 h (however, further consideration about this feature is complicated due to the low contrast issue in the micrographs) and the crystalline structure of the particle core can be observed from the phase contrast images (Fig. S16iii and iv†). In contrast, the materials collected at a longer reaction time of 84 h show the presence of structures of hundreds of nanometers, as observed in the low magnification images (Fig. S17i†). The high magnification images (Fig. S17ii–iv†) highlight the presence of the CD graphitic cores with an average diameter of around 6 nm that compose, with random orientation, the large polycrystalline aggregates.

The FTIR analysis (Fig. S18†) of the samples collected at different reaction times shows a significant increase in the absorption bands related to carboxylic acid functions, in particular, the υ_{O-H} 3500–2500 cm^{-1} and the υ_{CO} at 1720 cm^{-1} for the samples collected at 48 h and 84 h, respectively. This feature is followed by the reduction of the amidic bands (amide I and amide II at 1700 and 1590 cm^{-1}). Moreover, the sulfonic acid related absorption at 1030 cm^{-1} and the absence of signals of δ_{SH} at 941 cm^{-1} and υ_{CS} at 692 cm^{-1} show that the materials isolated at different reaction times contain sulfur in a high oxidation state, as expected by the oxidative reaction environment.[31]

We concluded that the chiroptical activity of the cysteine based chiral CDs produced by radical assisted decomposition originates from cysteine molecules or cysteine derivatives (amides, disulfide or sulfonic acid) grafted on the outer shell of the nanoparticles through amidic bonds. As shown in Fig. 8a and b, the ECD signal at 220 nm reaches a maximum between 1.5 and 2 h, which is associated with the formation of the maximum population of the chiral chromophores in the CD chiral shell. For reaction times longer than 2 h, the chiral information is progressively lost, a feature that can be related to the activity of decomposition processes that affects the grafted molecules which compose the "chiral shell" and give the formation of the inner structure such as achiral chromophores, luminophores and the graphitic core. This process can be related to the generation of the carbon centre radicals in the C_α position by the above-mentioned radical hydrogen transfer mechanisms that give the planarization of the stereocenter with the consecutive loss of chiral information. This hypothesis is supported by the UV/Vis and PL measurements, and our conclusions are in agreement with the observation on the chirality evolution for cysteine based CDs reported by others.[16,20] Finally, significant modifications in the CD morphology are observed only for the sample collected at a longer reaction time (84 h) probably due to an aggregation process that takes place when the functional groups present in the outer amorphous shells are sufficiently decomposed. Since the optical chirality and luminescence seems to follow an opposite trend in this system, it is necessary to consider which properties suit best the interest for a specific application in order to design the appropriate synthesis. Shorter reaction times maintain the chiral structures and give a higher chiroptical activity; on the other hand, longer reaction times promote the formation of luminophore rich structures at the expense of chiroptically active groups.

Conclusions

In this investigation, we present a new room temperature approach for the synthesis of cysteine based chiral CDs. The investigations on the mechanism involved in the nanoparticle formation suggest the role of the multivalent transition metal (copper) as a catalyst in the generation of radical species (ROS and RSS) that are active in the decomposition of the organic substrate. Moreover, by analysing the reactivity of similar substrates, we explore the role of carbon centre radicals in the nanoparticle formation. These findings can be a useful guideline in the design of new synthetic strategies for CDs based on radical assisted processes. The observations on the reactivity of different organic substrates have highlighted the formation of carbon centre radicals *via* radical hydrogen transfer reactions as fundamental processes involved in the formation of the CDs *via* this approach. The investigation on the chirality evolution during the reaction course reveals the fundamental details on the origin of these properties and the relationship with the nanoparticle structure.

Experimental section

Materials

L-Cysteine (98%) and D-cysteine (98%) were purchased from Alfa Aesar. L-Penicillamine (99%), cysteamine (95%), $Cu(OAc)_2$ (99%), deuterium oxide (99.9%), thioglycolic acid (98%), glycine (99%), sodium hydroxide, and hydrochloric acid (37%) were purchased from Sigma-Aldrich. All the chemicals were used without further purification.

Synthesis

1.24 mmol of L- or D-cysteine was solubilized in 100 mL of deionized water. The pH of the solution was adjusted to 10.5 with the addition of some drops of 2 M NaOH solution. Then, 0.200 mL of 0.25 M $Cu(OAc)_2$ solution (50 μmol) was added under vigorous stirring. The reaction mixture was kept under stirring at room temperature for 2.0 h. Then, the reaction was quenched by adjusting the pH below 7 with the addition of a few drops of 2 M HCl solution. At acidic pH, the by-product precipitates and it was removed by centrifugation (5000 rpm, 5 min). The supernatant was collected and purified by dialysis (3500 kDa, 24 h). The solvent was removed by vacuum distillation at room temperature to obtain a brown power. The CD dis-

persion with 1 mg ml^{-1} concentration in MilliQ water was prepared for the spectrophotometric analysis. The by-product fraction was dried under vacuum at room temperature to obtain a black powder. The by-product dispersion with 1 mg ml^{-1} in MilliQ water was prepared by adding NaOH to adjust the pH around 7.

Characterization

A ThermoFisher Talos FEI TEM was employed for the TEM analysis working with a 300 kV electron beam. A Zeiss Sigma VP field emission scanning electron microscope (FE-SEM) was employed for the SEM analysis and a Bruker Quantax 200 analyser was employed for the EDS analysis. UV/Vis analysis was carried out using an Agilent Cary 60 UV/Vis spectrophotometer. IR spectra were recorded using a NEXUS-FTIR instrument implementing a Nicolet diffuse reflectance infrared sampling accessory (DRIFT). A Panalytical Advanced powder diffractometer was employed for the XRD analysis. PL and PLE measurements were performed using a Jasco FP-8200 spectrofluorometer. Quantum yield measurements were performed with a Nanolog/Fluorolog-3-2iHR320 (Horiba-Jobin Yvon) spectrometer. Quinine sulfate (QS) 0.1 M acid sulfuric solution (quantum yield 0.54) was chosen as the standard. The quantum yield Y was obtained according to the following equation:[48]

$$Y_{CDs} = Y_{QS} \times \frac{F_{CDs}}{F_{QS}} \times \frac{A_{QS}}{A_{CDs}}$$

where F_{CDs} and F_{QS} are the measured integrated emission intensities, and A_{CDs} and A_{QS} are the optical density of CDs and QS, respectively. In order to minimize the reabsorption effect, absorption was kept below 0.10 at the excitation wavelength (350 nm).

Circular dichroism spectra were recorded using a Jasco spectropolarimeter J1500. ^{1}H-NMR data were acquired using a Bruker 300 MHz NMR spectrometer in D_2O. XPS measurements were performed using a PerkinElmer Φ 5600ci spectrometer, working in the 10^{-7} Pa pressure range at room temperature with nonmonochromatic Al K_α radiation (1486.6 eV). The BE values are referred to the Fermi level.

Conflicts of interest

There are no conflicts to declare.

Acknowledgements

The authors acknowledge “Centro Piattaforme Tecnologiche”, University of Verona, Italy, for the circular dichroism spectroscopy measurements. Financial support from the framework of “Joint Projects 2018”, University of Verona, Italy, is gratefully acknowledged.

References

1 V. Georgakilas, J. A. Perman, J. Tucek and R. Zboril, *Chem. Rev.*, 2015, **115**, 4744–4822.
2 K. Nekoueian, M. Amiri, M. Sillanpaa, F. Marken, R. Boukherroub and S. Szunerits, *Chem. Soc. Rev.*, 2019, **48**, 4281–4316.
3 S. Y. Lim, W. Shen and Z. Gao, *Chem. Soc. Rev.*, 2015, **44**, 362–381.
4 O. S. Wolfbeis, *Chem. Soc. Rev.*, 2015, **44**, 4743–4768.
5 Y. Sun, B. Zhou, Y. Lin, W. Wang, K. A. S. Fernando, P. Pathak, M. J. Meziani, B. A. Harruff, X. Wang, H. Wang, P. G. Luo, H. Yang, M. E. Kose, B. Chen, L. M. Veca and S. Xie, *J. Am. Chem. Soc.*, 2006, **128**, 7756–7757.
6 S. Cailotto, E. Amadio, M. Facchin, M. Selva, E. Pontoglio, F. Rizzolio, P. Riello, G. To, A. Benedetti and A. Perosa, *ACS Med. Chem. Lett.*, 2018, **9**, 832–837.
7 A. Emanuele, S. Cailotto, C. Campalani, L. Branzi, C. Raviola, D. Ravelli, E. Cattaruzza, E. Trave, A. Benedetti, M. Selva and A. Perosa, *Molecules*, 2020, **25**, 101.
8 H. Song, M. Wu, Z. Tang, J. S. Tse, B. Yang and S. Lu, *Angew. Chem.*, 2021, **60**, 7234–7244.
9 J. Liu, R. Li and B. Yang, *ACS Cent. Sci.*, 2020, **6**, 2179–2195.
10 F. Li, D. Yang and H. Xu, *Chem. – Eur. J.*, 2019, **25**, 1165–1176.
11 Z. Tang, *Chiral Nanomaterials: Preparation, Properties and Application*, Wiley-VCH, Weinheim, Germany, 1st edn, 2018.
12 N. Suzuki, Y. Wang, P. Elvati, Z. Qu, K. Kim, S. Jiang, E. Baumeister, J. Lee, B. Yeom, J. H. Bahng, J. Lee, A. Violi and N. A. Kotov, *ACS Nano*, 2016, **10**, 1744–1755.
13 M. Vázquez-Nakagawa, L. Rodriguez-Pérez, M. A. Herranz and N. Martín, *Chem. Commun.*, 2016, **52**, 665–668.
14 Y. Zhang, L. Hu, Y. Sun, C. Zhu, R. Li, N. Liu, H. Huang, Y. Liu, C. Huang and Z. Kang, *RSC Adv.*, 2016, **6**, 59956–59960.
15 L. Hu, Y. Sun, Y. Zhou, L. Bai, Y. Zhang, M. Han, H. Huang, Y. Liu and Z. Kang, *Inorg. Chem. Front.*, 2017, **4**, 946–953.
16 L. Hu, H. Li, C. Liu, Y. Song, M. Zhang, H. Huang, Y. Liu and Z. Kang, *Nanoscale*, 2018, **10**, 2333–2340.
17 M. Zhang, L. Hu, H. Wang, Y. Song, Y. Liu, H. Li, M. Shao, H. Huang and Z. Kang, *Nanoscale*, 2018, **10**, 12734–12742.
18 F. Li, Y. Li, X. Yang, X. Han, Y. Jiao, T. Wei, D. Yang, H. Xu and G. Nie, *Angew. Chem., Int. Ed.*, 2018, **57**, 2377–2382.
19 F. Li, S. Li, X. Guo, Y. Dong, C. Yao, Y. Liu, Y. Song, X. Tan, L. Gao and D. Yang, *Angew. Chem.*, 2020, **59**, 11087–11092.
20 F. Victoria, J. Manioudakis, L. Zaroubi, B. Findlay and R. Naccache, *RSC Adv.*, 2020, **10**, 32202–32210.
21 Y. Wei, L. Chen, J. Wang and X. Liu, *RSC Adv.*, 2019, **9**, 3208–3214.
22 L. Đorđević, F. Arcudi, A. D. Urso, M. Cacioppo, N. Micali, T. Bürgi, R. Purrello and M. Prato, *Nat. Commun.*, 2018, **9**, 3342.
23 D. Qu and Z. Sun, *Mater. Chem. Front.*, 2020, **4**, 400–420.
24 M. J. Krysmann, A. Kelarakis, P. Dallas and E. P. Giannelis, *J. Am. Chem. Soc.*, 2012, **134**, 747–750.

25 J. Schneider, C. J. Reckmeier, Y. Xiong, M. Von Seckendor, A. S. Susha and A. L. Rogach, *J. Phys. Chem. C*, 2017, **121**, 2014–2022.
26 Y. Song, S. Zhu, S. Zhang, Y. Fu, L. Wang, X. Zhao and B. Yang, *J. Mater. Chem. C*, 2015, **3**, 5976–5984.
27 M. J. Davies, *Biochim. Biophys. Acta*, 2005, **1703**, 93–109.
28 H. Sies, *Angew. Chem., Int. Ed. Engl.*, 1986, **25**, 1058–1071.
29 A. V. Kachur, C. J. Koch and J. E. Biaglow, *Free Radical Res.*, 1999, **31**, 23–34.
30 A. Pawlukojć, J. Leciejewicz, A. J. Ramirez-Cuesta and J. Nowicka-Scheibe, *Spectrochim. Acta, Part A*, 2005, **61**, 2474–2481.
31 G. Socrates, *Infrared and Raman Characteristic Group Frequencies Contents*, John Wiley & Sons Ltd., Baffis Lane, 3rd edn, 2001.
32 M. Fu, F. Ehrat, Y. Wang, K. Z. Milowska, C. Reckmeier, A. L. Rogach, J. K. Stolarczyk, A. S. Urban and J. Feldmann, *Nano Lett.*, 2015, **15**, 6030–6035.
33 S. Do, W. Kwon, Y. Kim, S. R. Kang, T. Lee, T. Lee and S. Rhee, *Adv. Opt. Mater.*, 2016, **4**, 276–284.
34 T. Yoshinaga, Y. Iso and T. Isobe, *J. Lumin.*, 2019, **213**, 6–14.
35 N. Amdursky and M. M. Stevens, *ChemPhysChem*, 2015, **16**, 2768–2774.
36 J. Yu, C. Xu, Z. Tian, Y. Lin and Z. Shi, *New J. Chem.*, 2016, **40**, 2083–2088.
37 T. Nauser, W. H. Koppenol and C. Schöneich, *J. Phys. Chem. B*, 2012, **116**, 5329–5341.
38 A. P. Mathews and S. Walker, *J. Biol. Chem.*, 1909, **6**, 299–312.
39 G. A. Bagiyan, I. K. Koroleva, N. V. Soroka and A. V. Ufimtsev, *Russ. Chem. Bull. Int. Ed.*, 2003, **52**, 1135–1141.
40 L. Pecci, G. Montefoschi, G. Musci, D. Cavallini, M. Cnr, L. Sapienza and U. Messina, *Amino Acids*, 1997, **13**, 355–367.
41 A. Rigo, A. Corazza, M. Luisa, M. Rossetto, R. Ugolini and M. Scarpa, *J. Inorg. Biochem.*, 2004, **98**, 1495–1501.
42 M. Buzuk, S. Brinić, N. Vladislavić, M. Bralić, M. Buljac and I. S. Rončević, *Monatsh. Chem.*, 2016, **147**, 359–367.
43 G. A. Bagiyan, I. K. Koroleva, N. V. Soroka and A. V. Ufimtsev, *Kinet. Catal.*, 2004, **45**, 398–406.
44 D. Cavallini, C. De Marco, S. Duprè and G. Rotilio, *Arch. Biochem. Biophys.*, 1969, **130**, 354–361.
45 R. Zhao, J. Lind, G. Merbnyi and T. E. Eriksen, *J. Am. Chem. Soc.*, 1994, **116**, 12010–12015.
46 S. D. Abramovitch and J. Rabani, *J. Phys. Chem.*, 1976, **80**, 1562–1565.
47 A. Hanaki, *Chem. Pharm. Bull.*, 1974, **22**, 2491–2492.
48 L. Hu, Y. Sun, S. Li, X. Wang, K. Hu, L. Wang, X. Liang and Y. Wu, *Carbon*, 2014, **67**, 508–513.